scientific reports

Check for updates

OPEN

Green synthesis of silver nanoparticles from *Buddleja asiatica* L. and their multifunctional applications for industrial and bio-based products

Maryum Fatima[1], Muhammad Shoaib Amjad[2,3], Ansar Mehmood[4], Samiullah Khan[1], Zakia Binish[2], Huma Arshad[5], Huma Qureshi[6], Tauseef Anwar[7]✉, Hossam S. El-Beltagi[8]✉, Ibtisam M. Alsudays[9], Khalid H. Alamer[10], Nazih Y. Rebouh[11] & Mohd Asif Shah[12,13,14]✉

Nanotechnology provides innovative solutions to biomedical and agricultural challenges, and silver nanoparticles (AgNPs) are of particular interest due to their broad-spectrum bioactivity. This study aimed to green-synthesize AgNPs using *Buddleja asiatica* leaf extract, characterize the nanoparticles, and evaluate antibacterial, antioxidant, anticancer, and phytotoxic/phytostimulatory activities. AgNP formation was confirmed by UV–visible spectroscopy (SPR peak at 420 nm). XRD verified a crystalline face-centered cubic structure, while SEM showed predominantly near-spherical nanoparticles (10–22 nm). FTIR indicated plant-derived functional groups involved in stabilization. Biologically, BA-AgNPs exhibited strong antibacterial activity against a Gram-positive clinical isolate (*Streptococcus* sp.) and Gram-negative bacteria, with the largest inhibition zone of 14 ± 0.57 mm at 0.9 mg/mL. Antioxidant activity reached 88.12% DPPH scavenging at 100 ppm, compared with 80.90% for ascorbic acid under the same assay conditions. BA-AgNPs showed concentration-dependent cytotoxicity in RD cells, with cell death ranging from 87.00% at 100 mg/mL to 5.33% at 0.39062 mg/mL; however, IC_{50} is reported only as an estimated range of 6.25–12.5 mg/mL based on the concentration interval where cytotoxicity crossed 50%. In wheat, lower concentrations showed phytostimulatory trends, with the strongest response at 50 mg/L, while 1000 mg/L caused inhibitory effects. This is the first comprehensive report on *B. asiatica*–mediated AgNP synthesis and multifunctional bioactivity, highlighting BA-AgNPs as a sustainable nanomaterial for antimicrobial, antioxidant, anticancer, and agricultural applications, while emphasizing the need for future stability, mechanistic, and translational safety studies.

Keywords SIlver nanoparticles, Green synthesis, *Buddleja asiatica*, Antibacterial, Antioxidant, Anticancer, Phytotoxicity

[1]Department of Botany, Women University of Azad Jammu and Kashmir, Bagh, Azad Kashmir 12500, Pakistan. [2]Department of Botany, University of Kotli, Azad Jammu and Kashmir, Kotli 11100, Pakistan. [3]Birmingham Institute of Forest Research, University of Birmingham, Birmingham B15 2TT, UK. [4]Department of Botany, University of Poonch, Rawalakot 12350, Pakistan. [5]Department of Plant Sciences, Quaid-e-Azam University, Islamabad 45320, Pakistan. [6]Department of Botany, University of Chakwal, Chakwal 48800, Pakistan. [7]Department of Botany, The Islamia University of Bahawalpur, Bahawalpur 63100, Pakistan. [8]Agricultural Biotechnology Department, College of Agriculture and Food Sciences, King Faisal University, 31982 Al-Ahsa, Saudi Arabia. [9]Department of Biology, College of Science, Qassim University, Qassim, Saudi Arabia. [10]Biological Sciences Department, Faculty of Science and Arts, King Abdulaziz University, Rabigh 21911, Saudi Arabia. [11]Institute of Environmental Engineering, RUDN University, Miklukho-Maklaya St, Moscow, Russia117198. [12]Kardan University, Parwane Du 1001, Kabul, Afghanistan. [13]Division of Research and Development, Lovely Professional University, Phagwara, Punjab 144001, India. [14]University Centre for Research & Development, Chandigarh University, Gharuan, Mohali, Punjab 140413, India. ✉email: tauseef.anwar@iub.edu.pk; helbeltagi@kfu.edu.sa; m.asif@kardan.edu.af

Nanotechnology has emerged as a transformative field focused on the design and application of nanomaterials for diverse sectors, including biomedicine, pharmaceuticals, catalysis, agriculture, food technology, sensing, and environmental remediation[1,2]. Nanoparticles, defined as materials with at least one dimension below 100 nm, exhibit unique physicochemical, optical, and biological properties arising from their high surface area-to-volume ratio, tunable surface chemistry, and enhanced reactivity[3,4]. These attributes have enabled their widespread use as antibacterial, anticancer, and antiviral agents[5–7].

Among metallic nanomaterials, silver nanoparticles (AgNPs) are among the most extensively investigated owing to their broad-spectrum antimicrobial activity, chemical stability, and capacity to release bioactive silver ions that induce oxidative stress and disrupt microbial cellular processes[8,9]. AgNPs have demonstrated promising applications in combating multidrug-resistant pathogens, inhibiting biofilm formation, enhancing wound healing, and serving as drug delivery platforms in cancer therapy[10–12]. Beyond biomedical uses, AgNPs are increasingly explored in water purification, catalysis, sensing technologies, and agriculture[13–15].

AgNPs can be synthesized using physical, chemical, and biological methods; however, conventional chemical and physical routes often require toxic reagents, high energy input, and harsh reaction conditions, raising environmental and health concerns[16–18]. Consequently, green synthesis approaches employing biological systems—particularly plant extracts—have gained substantial attention as sustainable alternatives. Plant-mediated synthesis is cost-effective, scalable, and environmentally benign, while simultaneously enabling phytochemicals to act as reducing, stabilizing, and capping agents that influence nanoparticle size, morphology, surface charge, and biological performance[19–21].

Buddleja asiatica (family Scrophulariaceae) is an ornamental and medicinal plant widely distributed across Africa, Asia, and the Americas. It is traditionally used for treating inflammatory disorders, infections, skin ailments, fever, and pain, and is known to possess antimicrobial, antifungal, antioxidant, and cytotoxic properties[22–24]. Phytochemical investigations of the *Buddleja* genus have reported the presence of flavonoids, phenylethanoids, lignans, neolignans, terpenoids, and saponins, many of which are biologically active and capable of participating in redox reactions[25,26]. These characteristics make *B. asiatica* a promising candidate for green nanoparticle synthesis. Recent studies further demonstrate the growing relevance of green-synthesized and biofunctional nanoparticles in antimicrobial, antioxidant, anticancer, catalytic, and agricultural applications. For example, recent nanoparticle studies have emphasized the importance of synthesis route, capping chemistry, size distribution, surface charge, and biological test conditions in determining nanoparticle performance[27–30]. Therefore, comparison with recent nanoparticle studies is essential for positioning BA-AgNPs within current nanobiotechnology research and for identifying gaps related to stability, reproducibility, safety, and mechanistic validation.

In plant-mediated nanoparticle synthesis, functional groups detected by FTIR provide evidence of biomolecule involvement in metal ion reduction and nanoparticle stabilization; however, FTIR alone does not identify the specific phytochemicals responsible for these processes. While flavonoids, polyphenols, terpenoids, and related metabolites are widely reported as key reducing and capping agents, definitive attribution requires targeted phytochemical profiling using advanced analytical techniques such as HPLC–MS or GC–MS. The present study relies on FTIR-based functional group analysis to confirm biomolecular participation but does not identify individual compounds responsible for silver ion reduction and stabilization. This limitation is acknowledged, and comprehensive phytochemical characterization of *B. asiatica* extract before and after nanoparticle synthesis is recommended for future work to fully elucidate the mechanistic basis of the green synthesis process.

To the best of our knowledge, this is the first report describing the green synthesis of silver nanoparticles using *B. asiatica* leaf extract. The objectives of this study were (i) to synthesize and physicochemically characterize *B. asiatica*–mediated AgNPs, and (ii) to evaluate their antibacterial, antioxidant, anticancer, and phytotoxic/phytomodulatory activities. By integrating green synthesis with biological performance assessment, this work provides foundational insight into the potential of *B. asiatica*–derived AgNPs for biomedical and agricultural applications, while also identifying critical areas for further mechanistic and translational investigation.

Materials and methods

Collection of plant material

Fresh leaves of *Buddleja asiatica* L. were collected from healthy plants growing in Dhirkot, District Bagh, Azad Jammu & Kashmir, Pakistan. The plant material was formally identified by Dr. Muhammad Shoaib Amjad, Assistant Professor, Department of Botany, University of Kotli, Azad Jammu and Kashmir, Kotli 11,100, Pakistan. A voucher specimen was prepared and deposited in the Herbarium of the Department of Botany, University of Kotli, Azad Jammu and Kashmir, Pakistan, under voucher number 587942, where it is available for future reference and public access. Permission for plant collection was obtained, and all procedures involving plant material were conducted in accordance with relevant institutional, national, and international guidelines.

Chemicals and reagents

Silver nitrate ($AgNO_3$;analytical grade, ≥ 99% purity), 2,2-diphenyl-1-picrylhydrazyl (DPPH; analytical grade), ascorbic acid (analytical grade), methanol (analytical grade), acetone (analytical grade), potassium bromide (KBr; spectroscopy grade), and sodium hypochlorite solution were purchased from Sigma-Aldrich, USA, unless otherwise stated. 3-(4,5-dimethylthiazol-2-yl)-2,5-diphenyltetrazolium bromide (MTT; cell-culture grade), Eagle's Minimum Essential Medium, and other cell-culture reagents were obtained from Thermo Fisher Scientific/Gibco, USA. Mueller–Hinton agar was obtained from Oxoid, UK. Distilled/deionized water was used throughout the synthesis, washing, dilution, and assay procedures. All chemicals and reagents were used without further purification.

Preparation of leaf extract

Collected leaves were washed twice with tap water to remove surface contaminants, followed by three rinses with distilled water. The cleaned leaves were shade-dried at ambient temperature for 21 days and then ground into a fine powder using an electric grinder. Ten grams of powdered leaf material were mixed with 100 mL of deionized water in a 250 mL conical flask and maintained at room temperature for 72 h with intermittent shaking. The mixture was filtered through Whatman No. 1 filter paper, and the aqueous filtrate was stored at 4 °C for use in nanoparticle synthesis[31,32].

Biosynthesis of silver nanoparticles

Silver nanoparticles were synthesized via a green reduction approach using *B. asiatica* leaf extract as the reducing and stabilizing agent. Briefly, 20 mL of aqueous leaf extract was mixed with 80 mL of 1 mM $AgNO_3$ solution (Sigma-Aldrich, USA) under aseptic conditions. The reaction mixture was maintained at room temperature and incubated in the dark for 24 h to minimize any photoinduced reduction of silver ions. In the present study, the synthesis protocol was carried out under a fixed set of reaction parameters, and no systematic optimization was performed with respect to reaction temperature or precursor concentration. Specifically, the effects of varying temperature and $AgNO_3$ molarity on nanoparticle formation efficiency, conversion yield, or particle characteristics were not evaluated. After incubation, the reaction suspension was centrifuged at 10,000 rpm for 10 min to recover the nanoparticulate fraction. The resulting pellet was washed twice with distilled water and once with acetone to remove unbound phytochemical residues and excess precursor, followed by freeze-drying and grinding to obtain dried AgNP powder for downstream characterization and bioactivity assays[33,34].

Characterization of silver nanoparticles

UV–visible spectroscopy

Formation of AgNPs was monitored using UV–visible spectroscopy. Absorbance spectra of the colloidal suspension were recorded over a wavelength range of 300–700 nm using a PerkinElmer Lambda 950 UV–Vis spectrophotometer, with distilled water as the reference. In the present study, the spectrum reported in Fig. 2 was recorded after 24 h of incubation, corresponding to the endpoint of the synthesis reaction; intermediate time-point spectra were not collected[35].

X-ray diffraction (XRD)

Crystallographic analysis of AgNPs was performed using a Bruker D8 X-ray diffractometer[36]. Freeze-dried nanoparticle powder was mounted on the sample holder and analyzed by 2θ scanning. Diffraction peaks were indexed by comparison with standard reference data for face-centered cubic (fcc) metallic silver (JCPDS card no. 04–0783). Crystallite size was estimated using the Debye–Scherrer equation.

$$D = K\lambda / (\beta \cos\theta) \quad (1)$$

where K is the shape factor, λ is the X-ray wavelength, β is the full width at half maximum (FWHM) expressed in radians, and θ is the Bragg angle. Instrumental broadening correction was not applied; therefore, Scherrer-derived values are reported as approximate crystallite-domain estimates.

Scanning electron microscopy (SEM) and energy dispersive X-ray (EDX)

Surface morphology and particle size distribution were examined using a JEOL JSM-6490A scanning electron microscope. AgNPs were dispersed in distilled water and drop-cast onto a conductive carbon-coated support suitable for SEM imaging, then air-dried prior to analysis. Elemental composition was confirmed using EDX analysis coupled with SEM. Particle size distribution was quantified using ImageJ software from SEM micrographs.

Fourier transform infrared spectroscopy (FTIR)

FTIR analysis was performed to identify functional groups involved in AgNP reduction and stabilization. Freeze-dried samples were mixed with potassium bromide (KBr), pelletized, and analyzed using a PerkinElmer Spectrum GX FT-IR spectrometer over the range of 400–4000 cm^{-1} at a resolution of 4 cm^{-1} [37,38].

Zeta potential analysis

Zeta potential measurements were carried out using a HORIBA SZ-100 analyzer to determine surface charge and colloidal stability of the synthesized AgNPs[39].

Biological activities

Antibacterial activity

Antibacterial activity of AgNPs was evaluated using the agar well diffusion method[40] against *Klebsiella pneumoniae*, *Streptococcus* sp., *Escherichia coli*, and *Pseudomonas aeruginosa*. Bacterial strains were obtained from CMH Rawalakot. Mueller–Hinton agar was prepared, sterilized by autoclaving at 121 °C for 15 min, and the plates were inoculated with bacterial suspension. Wells were loaded with AgNPs at concentrations of 0.1, 0.3, 0.5, 0.7, and 0.9 mg/mL. Ampicillin (0.1%) served as the positive control, while distilled water was used as the negative control. Plates were incubated at 37 °C for 48 h, and zones of inhibition were measured in millimeters. Plant extract alone was not tested as a separate control in the antibacterial assay. Therefore, the present results specifically demonstrate the activity of the BA-AgNP formulation, while the independent contribution of the crude plant extract remains unresolved. This limitation is acknowledged, and future assays will include extract-only controls to distinguish nanoparticle-mediated activity from phytochemical-associated activity. The

experimental design was focused on determining the antimicrobial efficacy of the nanoparticle formulation. Comparative assessment of extract-only preparations will be undertaken in future studies to delineate the contributions of phytochemicals and metallic nanoparticles.

Antioxidant activity

Antioxidant activity of BA-AgNPs was assessed using the DPPH radical scavenging assay[41]. DPPH solution was prepared by dissolving 0.0125 g DPPH in 50 mL methanol and kept in the dark. AgNP solutions were prepared at concentrations of 10, 20, 40, 50, 75, and 100 ppm. Equal volumes (2 mL) of DPPH solution and AgNP solution were mixed and incubated for 30 min. Ascorbic acid was used as the standard. Absorbance was measured at 517 nm. Antioxidant activity was calculated using the equation:

$$\text{DPPH scavenging assay } (\%) = [(\text{A0} - \text{A1}) / \text{A0}] \times 100 \quad (2)$$

where A_0 is the absorbance of the control and A_1 is the absorbance of the sample.

Anticancer activity

Anticancer activity was evaluated using the MTT assay following Lyons et al.[42]. Rhabdomyosarcoma (RD) cells were obtained from the National Institute of Health, Islamabad, and maintained at PIEAS. Cells were cultured in Eagle's Minimum Essential Medium and incubated at 37 °C in a 5% CO_2 atmosphere. Each well of a 96-well plate was seeded with 5×10^3 cells and exposed to increasing concentrations of AgNPs for 24 h. MTT solution (10 µL, 5 mg/mL) was added and incubated for 3 h. Absorbance was measured at 595 nm. The anticancer assay consisted of the following groups: untreated RD cells as the negative/viability control, BA-AgNP-treated RD cells at different concentrations, and blank wells containing medium without cells for background correction. Each concentration was tested in triplicate. Cell viability/ cytotoxicity was validated by comparing treated wells with untreated control wells after MTT reduction, and the percentage of cell death was calculated from absorbance values after background correction. The present assay was designed as a preliminary cytotoxicity screening; therefore, nonlinear regression-based IC_{50} calculation was not performed. The IC_{50} was interpreted only as an estimated range between the two tested concentrations where cytotoxicity changed from below 50% to above 50%.

Cytotoxicity was calculated as:

$$\text{Proportion of dead cells } (\%) = [(\text{Y} - \text{X}) / \text{Y}] \times 100 \quad (3)$$

where Y is the absorbance of untreated cells and X is the absorbance of treated cells.

Leaf extract alone and non-cancerous mammalian cell-line controls were not tested for cytotoxicity in the present study. Therefore, the anticancer assay was limited to preliminary cytotoxic screening of BA-AgNPs against RD cancer cells, and selective anticancer efficacy cannot be confirmed from the current data. Because additional normal-cell experiments require new cell-culture work beyond the scope of this revision, the findings are interpreted cautiously as RD-cell cytotoxicity rather than confirmed cancer-selective activity. Future studies will include non-cancerous mammalian cell lines, such as fibroblast or epithelial cell models, together with extract-only controls, to calculate selectivity index, confirm biocompatibility, and distinguish selective anticancer activity from general cytotoxicity.

Phytotoxic analysis

Phytotoxic effects of AgNPs were assessed using wheat (*Triticum aestivum* var. Akbar 2019). Seeds were surface-sterilized with 3% sodium hypochlorite and sown in washed sand. Plants were maintained at 25 ± 1 °C. AgNPs were applied at concentrations of 25, 50, 100, and 1000 mg/L on the 8th day after germination. Root length, shoot length, and fresh biomass were recorded on days 9, 10, and 11. Experiments were conducted in triplicate.

Hemocompatibility assays and cytotoxicity evaluation using non-cancerous mammalian cell lines were not performed. The scope of this study was limited to synthesis, characterization, and preliminary biological screening. Comprehensive biocompatibility studies will be conducted in future work.

Statistical analysis

All experiments were performed in triplicate. Data were analyzed using one-way analysis of variance (ANOVA) and Student's t-test in SPSS software (version 22). Results were expressed as mean ± standard error of the mean (SEM). Different lowercase letters shown in graphs indicate statistically significant differences among treatments at $p < 0.05$.

Results and discussion

Green synthesis and optical confirmation of BA-AgNPs

Silver nanoparticles were synthesized using *Buddleja asiatica* leaf extract as a reducing and stabilizing agent by reacting it with 1 mM $AgNO_3$. A progressive color transition of the reaction mixture from transparent to yellowish and ultimately dark brown was observed within 24 h (Fig. 1). This visible change is a widely accepted preliminary indicator of AgNP formation in green synthesis systems and is primarily attributed to surface plasmon resonance (SPR) resulting from collective oscillation of conduction electrons following the reduction of Ag^+ to Ag^0[34,43,44].

UV–Vis spectroscopy further confirmed nanoparticle formation by displaying a characteristic SPR absorption band within the 400–500 nm region (Fig. 2). SPR peak position and band broadness are influenced by particle size distribution, morphology, aggregation state, and the surrounding dielectric environment[45]. The observed

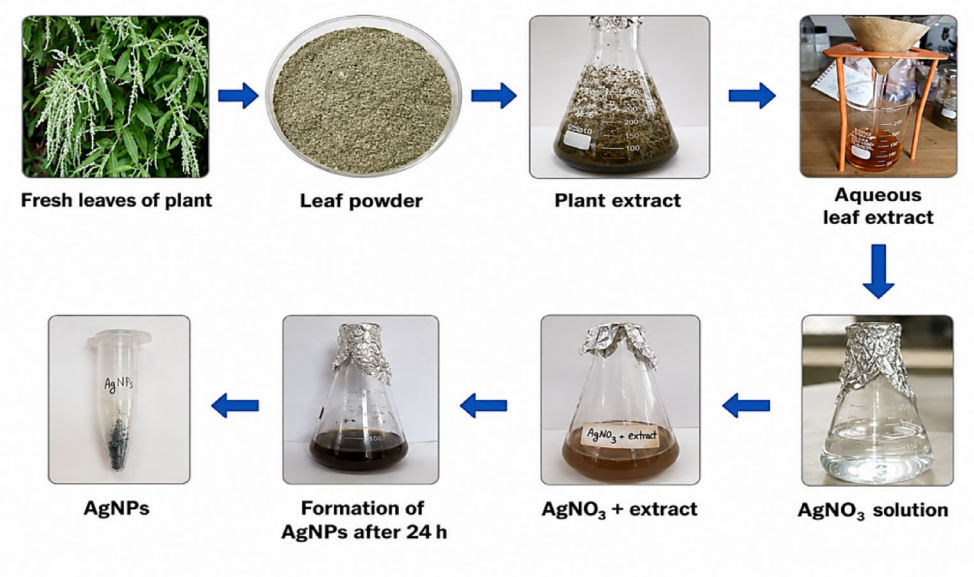

Fig. 1. Visual color change during green synthesis of BA-AgNPs. Reaction mixture containing *B. asiatica* leaf extract and 1 mM $AgNO_3$ incubated for 24 h at room temperature under dark conditions, showing progression from pale yellow to dark brown indicative of AgNPs formation.

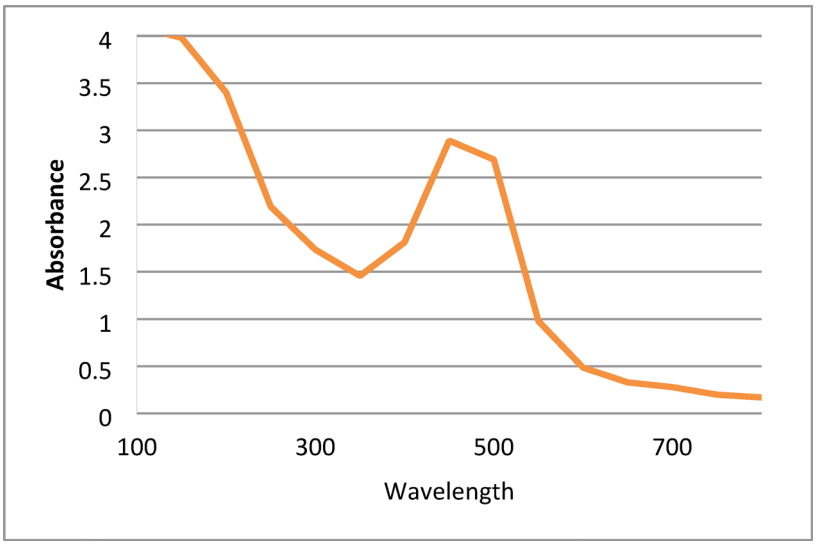

Fig. 2. UV–vis absorption spectrum of BA-AgNP colloid (300–700 nm) showing the characteristic surface plasmon resonance band with λ_max at ~ 420 nm.

SPR range is consistent with multiple reports on plant-mediated AgNPs, where absorbance maxima typically occur between 400 and 500 nm[34,44,46]. Comparable peaks have also been reported for AgNPs synthesized using *Cinnamomum camphora* (~ 420 nm)[47] and *Nigella sativa* (~ 400 nm)[48], supporting the optical behavior of BA-AgNPs reported here.

Structural, morphological, and surface chemistry characterization

XRD crystallinity and phase confirmation

X-ray diffraction (XRD) analysis verified the crystalline nature of BA-AgNPs (Fig. 3; Table 1). Four dominant diffraction peaks at $2\theta = 38.16°$, 43.00°, 65.00°, and 77.00° corresponded to the (111), (200), (220), and (311) lattice planes, respectively, confirming a face-centered cubic (fcc) silver structure. These peaks closely matched standard silver reference data (JCPDS card no. 04-0783), indicating high crystallinity and phase identification consistent with earlier reports of green-synthesized AgNPs[46,49]. The interplanar spacings (d) calculated from Bragg's law are presented in Table 1. Crystallite sizes were estimated using the Debye–Scherrer equation; however, Scherrer-derived values represent coherent diffraction-domain sizes and may differ from SEM particle

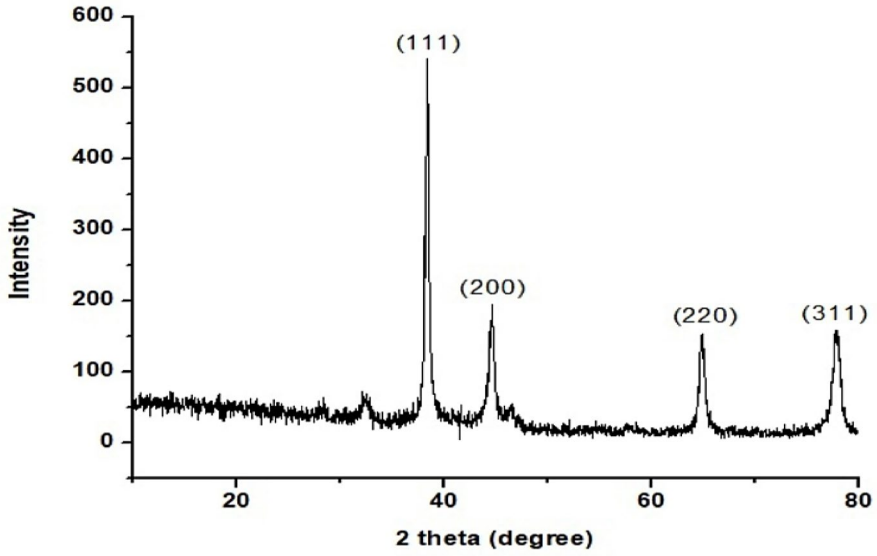

Fig. 3. XRD pattern of BA-AgNPs showing characteristic fcc silver reflections indexed to (111), (200), (220), and (311) planes (JCPDS 04-0783).

Reflection (hkl)	2θ (°)	Peak height (a.u.)	FWHM (°)	d-spacing (nm)	Relative intensity (a.u.)	Crystallite size (nm)
(111)	38.16	148.64	0.385	0.2356	100.12	21.8
(200)	43.00	40.86	0.624	0.2102	28.33	13.7
(220)	65.00	61.77	0.203	0.1434	41.13	46.4
(311)	77.00	52.68	0.645	0.1237	35.17	15.7

Table 1. XRD peak positions and crystallite size estimates for BA-AgNPs calculated using the Debye–Scherrer equation.

sizes due to aggregation, polycrystallinity, and the absence of instrumental broadening correction. Differences among reflections are commonly observed in plant-based synthesis due to preferential growth, crystallographic orientation, and phytochemical capping effects on crystal growth kinetics.

SEM morphology and size distribution

Scanning electron microscopy (SEM) revealed that BA-AgNPs were predominantly near-spherical with relatively uniform morphology (Fig. 4). Particle size estimation indicated nanoscale dimensions predominantly within the ~ 10–22 nm range, supporting the UV–Vis SPR behavior observed in the 400–500 nm region and aligning with prior studies reporting spherical AgNP morphologies from plant-mediated synthesis[44,50]. Spherical morphology is frequently associated with SPR bands in the 400–450 nm range, supporting agreement between SEM and UV–Vis observations[51,52].

Elemental validation by EDX

EDX analysis confirmed the elemental composition of the synthesized nanoparticles. Strong Ag-associated signals were detected in the typical 2.5–3.8 keV region, with a prominent peak around ~ 3 keV attributable to silver (Figs. 5 and 6). Quantitative ZAF analysis indicated silver as the dominant element (weight % ~ 87.11; atomic % ~ 46.82), with minor contributions from carbon and oxygen (Table 2), consistent with organic capping by plant-derived biomolecules and in agreement with previous reports[34,53].

FTIR functional groups and capping interpretation

FTIR analysis of BA-AgNPs (Fig. 7; Table 3) revealed several characteristic absorption bands at approximately 3293, 2914, 2838, 1618, 1316, and 1019 cm^{-1}, indicating the presence of phytochemical residues adsorbed on the nanoparticle surface. The intense band centered near 3293 cm^{-1} is assigned to hydrogen-bonded O–H stretching vibrations, with possible contribution from N–H stretching of amine or amide-containing biomolecules. The bands at 2914 and 2838 cm^{-1} are attributed to asymmetric and symmetric aliphatic C–H stretching vibrations, respectively, and therefore should not be assigned to carbonyl (C=O) functionality. In contrast, the absorption feature at 1618 cm^{-1} lies in a more plausible region for carbonyl-related vibrational contributions, particularly conjugated C=O stretching and/or amide I vibrations, although overlap with aromatic C=C skeletal vibrations cannot be excluded in a complex plant-derived matrix. The band at 1316 cm^{-1} is consistent with C–O stretching and/or O–H bending of phenolic, alcoholic, carboxylate, or ester-containing constituents, while the peak

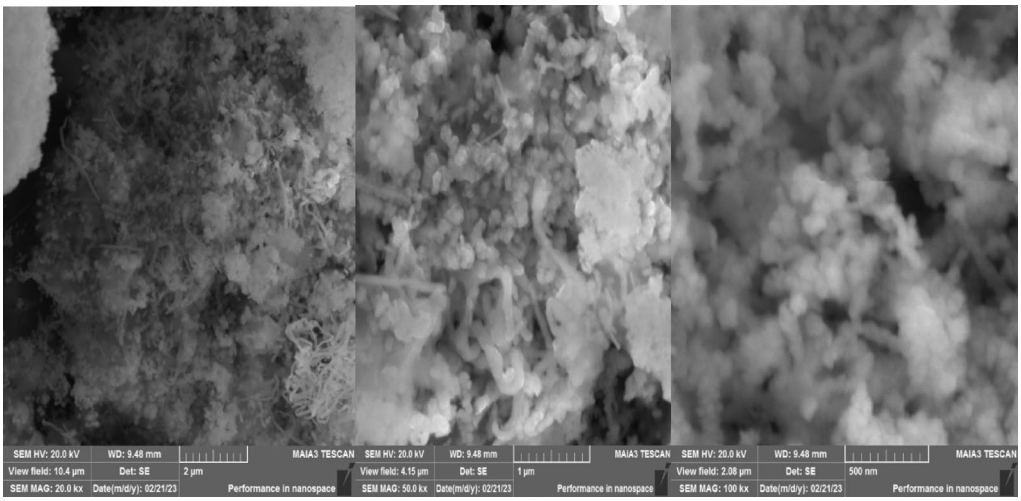

Fig. 4. SEM micrographs of BA-AgNPs at 20 K×, 50 K×, and 100 K× magnification showing predominantly near-spherical morphology and nanoscale dimensions.

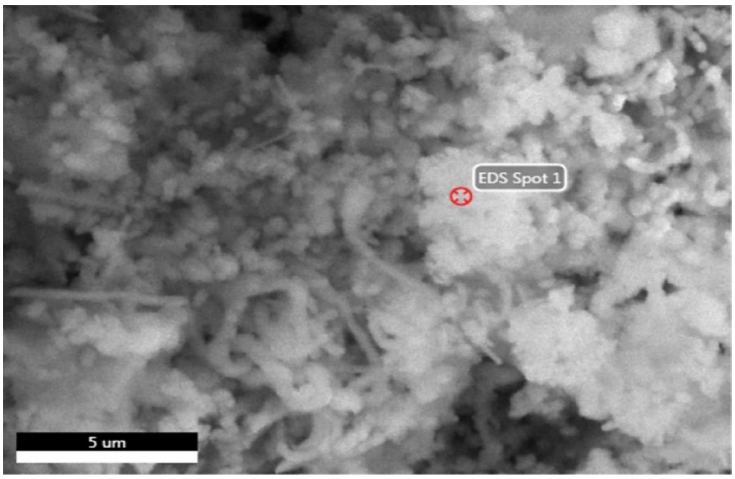

Fig. 5. SEM–EDX analysis of BA-AgNPs showing a dominant Ag signal (characteristic peak around ~ 3 keV) with minor C and O peaks consistent with organic capping and/or substrate contribution.

at 1019 cm^{-1} is assignable to C–N stretching and/or C–O stretching modes of biomolecules such as amino compounds, polysaccharides, or glycosidic residues.

Taken together, the FTIR profile supports the presence of polyphenolic, flavonoid, proteinaceous, and other oxygenated phytoconstituents associated with the BA-AgNP surface. These molecules likely played dual roles during synthesis, functioning both as electron-donating reductants for Ag^{+} conversion to Ag^{0} and as surface-capping agents that contribute to colloidal stabilization through steric and/or electrostatic effects. Because plant extracts represent chemically heterogeneous systems, all assignments should be regarded as tentative and based on characteristic band regions rather than definitive identification of individual compounds.

Zeta potential, dispersion stability, and identified limitation on long-term stability

Zeta potential provides an important indicator of electrostatic stabilization and dispersion behavior of colloidal nanoparticles. The BA-AgNPs showed a negative zeta potential of − 18.7 mV (Fig. 8; Table 4), indicating borderline electrostatic stability and suggesting that some aggregation risk may exist depending on ionic strength and storage conditions. The negative charge is consistent with association of anionic plant-derived biomolecules on the AgNP surface and is aligned with typical green-synthesized AgNP zeta potentials reported in the literature[39]. Comparable values have been reported for plant-extract-capped AgNPs, such as *Phyla dulcis* coated AgNPs (− 20 to − 24 mV)[54] and fungal-mediated AgNPs (~ − 20 mV)[55]. The negative charge may also influence bio-interactions because most mammalian and bacterial cell membranes carry a net negative charge, affecting electrostatic attraction/repulsion and cellular association dynamics[56].

Although BA-AgNPs displayed favorable initial surface charge and nanoscale dimensions, long-term colloidal stability was not evaluated in this study. Specifically, hydrodynamic diameter and polydispersity index

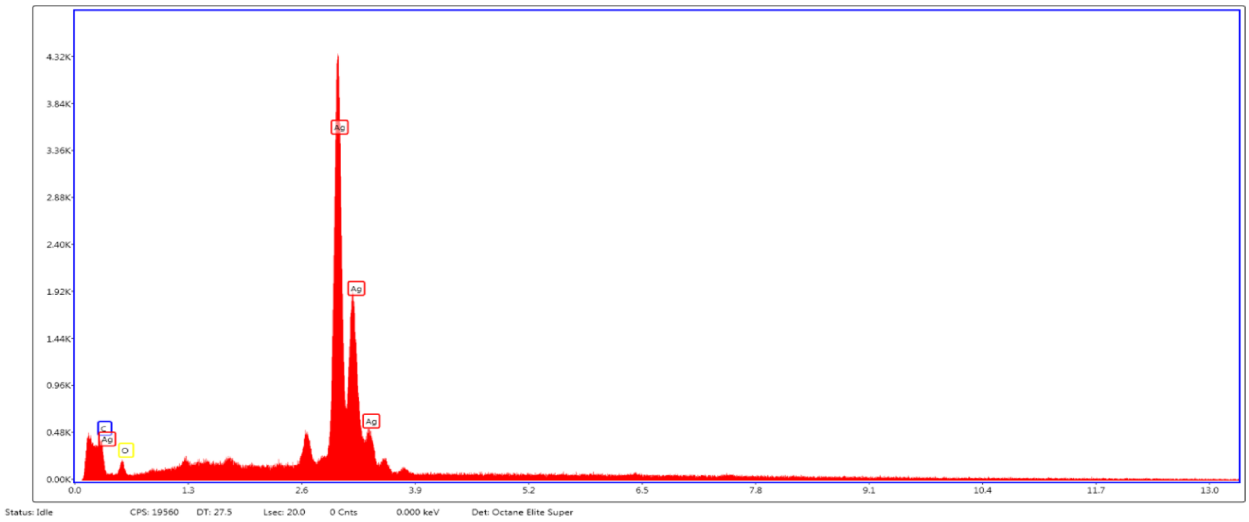

Fig. 6. EDX spectrum of BA-AgNPs showing elemental peaks and relative abundance.

Element (line)	Weight (%)	Atomic (%)	Net intensity	Error (%)	Kratio	Z	R	A	F
C (K)	7.17	33.90	263.97	6.19	0.0695	1.4029	0.7659	0.6902	1.0000
O (K)	5.72	20.28	59.61	17.19	0.0065	1.3487	0.7883	0.0842	1.0000
Ag (L)	87.11	46.82	4004.38	1.89	0.8547	0.9406	1.0474	1.0287	1.0140

Table 2. Elemental composition of BA-AgNPs determined by EDX (SEM–EDX).

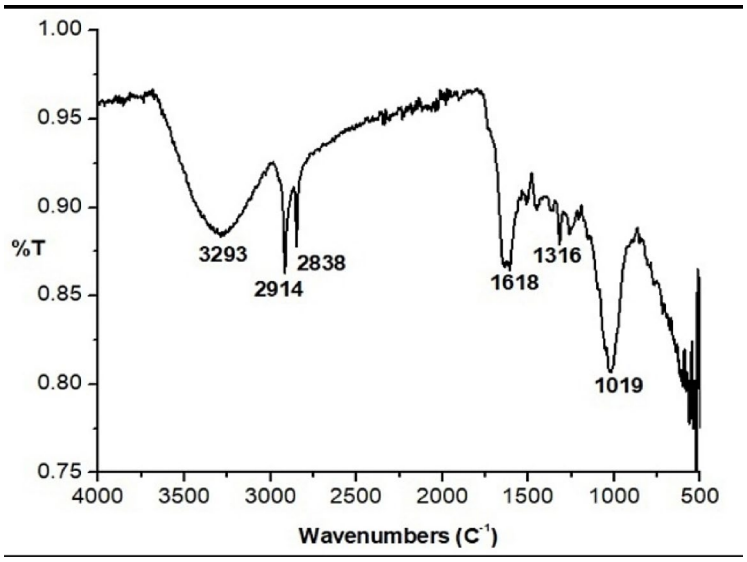

Fig. 7. FTIR spectrum of BA-AgNPs (400–4000 cm^{-1}) indicating functional groups associated with phytochemical capping and stabilization.

(DLS/PDI) were not measured at baseline or over storage time, and time-dependent changes in zeta potential after defined storage intervals (e.g., one week, one month, and three months) were not measured. Additionally, batch-to-batch consistency—an essential requirement for translation and industrial scale-up—was not assessed for size distribution and biological activity across independent synthesis batches. These are recognized limitations of the present work and require systematic evaluation in follow-up studies to confirm storage stability, shelf-life, and reproducibility of BA-AgNPs. Furthermore, since AgNP biological effects may arise from nanoparticle–cell interactions and/or released Ag^{+} ions, silver ion release kinetics into physiological media (e.g., PBS or cell culture media) over 24 h were not quantified in the current study. Such profiling is important to

FTIR band (cm^{-1})	Intensity	Tentative vibrational assignment	Likely functional groups/phytochemical origin
1019	Medium	C–N stretching and/or C–O stretching	Amines, alcohols, ethers, glycosidic residues
1316	Strong	C–O stretching and/or O–H bending	Phenolics, alcohols, carboxylates, esters
1618	Medium	Conjugated C=O stretching, amide I, and/or aromatic C=C skeletal vibration	Carbonyl-containing phytochemicals, proteins, aromatic compounds
2838	Medium	Symmetric aliphatic C–H stretching	$-CH_2/-CH_3$ groups of aliphatic constituents
2914	Medium	Asymmetric aliphatic C–H stretching	$-CH_2/-CH_3$ groups of aliphatic constituents
3293	Narrow, strong	Hydrogen-bonded O–H stretching with possible N–H contribution	Phenolics, alcohols, amines, proteins

Table 3. Major FTIR absorption bands of BA-AgNPs and tentative functional group assignments associated with phytochemical capping/stabilization.

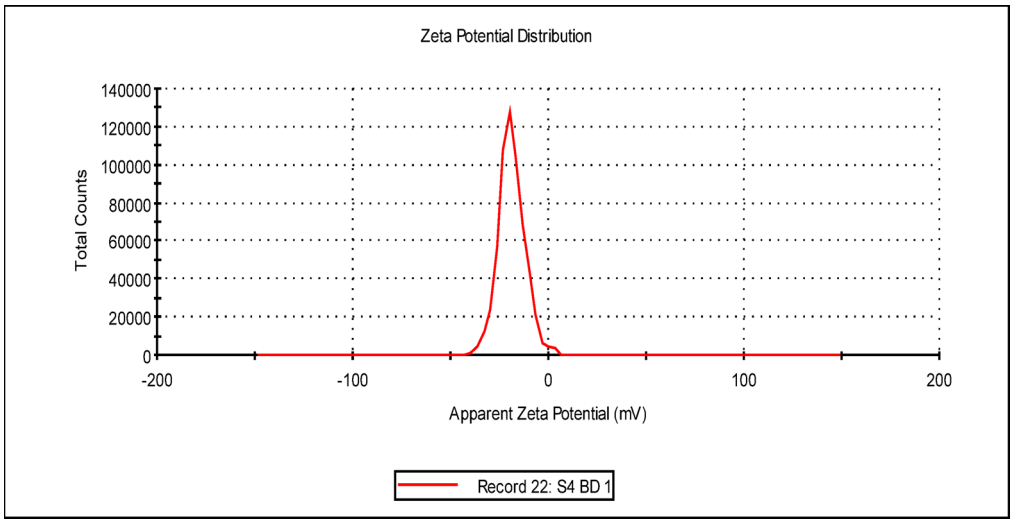

Fig. 8. Zeta potential distribution of BA-AgNPs measured in distilled water showing a mean zeta potential of − 18.7 mV, indicating borderline electrostatic stability.

Parameter	Result
Zeta potential (mean, mV)	− 18.7
Zeta deviation (SD, mV)	6.76
Peak 1 (mV); Area (%)	− 18.7; 100.0
Peak 2 (mV); Area (%)	0.00; 0.0
Peak 3 (mV); Area (%)	0.00; 0.0
Conductivity (mS/cm)	0.028
Result quality	Good

Table 4. Zeta potential of BA-AgNPs measured in distilled water (instrument: HORIBA SZ-100).

distinguish nanoparticle-driven effects from ion-mediated contributions and will be included in future work to strengthen mechanistic interpretation and support biomedical/industrial relevance[57–59]. In comparison with recent nanoparticle studies, the present BA-AgNPs show comparable multifunctional potential but also share common translational limitations, including incomplete long-term stability profiling, limited mechanistic validation, and the need for broader safety testing. Recent work has emphasized that biofunctional nanoparticles require not only physicochemical characterization but also reproducibility assessment, hydrodynamic size/PDI measurement, ion-release evaluation, and biological safety screening[27–30]. The current study therefore provides useful preliminary evidence for BA-AgNP bioactivity, while future work should follow these recent methodological standards to strengthen mechanistic and applied relevance.

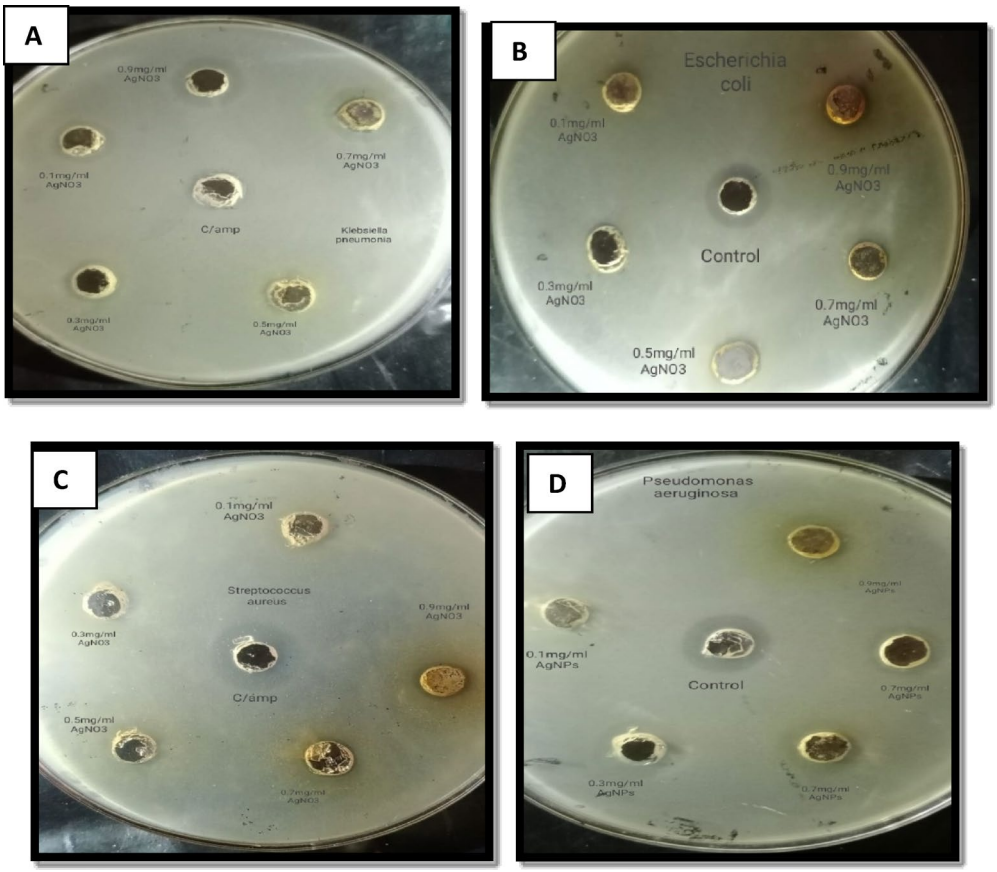

Fig. 9. Representative agar well diffusion plates showing inhibition zones produced by BA-AgNPs at different concentrations against bacterial strains: (**A**) *Klebsiella pneumoniae*, (**B**) *Escherichia coli*, (**C**) *Streptococcus* sp., and (**D**) *Pseudomonas aeruginosa*. Ampicillin was used as the positive control and distilled water as the negative control.

Bacterial species	BA-AgNPs 0.1 mg/mL (mm)	BA-AgNPs 0.3 mg/mL (mm)	BA-AgNPs 0.5 mg/mL (mm)	BA-AgNPs 0.7 mg/mL (mm)	BA-AgNPs 0.9 mg/mL (mm)	Ampicillin (0.1%) (mm)
Klebsiella pneumoniae	5.66 ± 1.49	6.00 ± 1.25	6.93 ± 0.92	7.50 ± 1.50	12.33 ± 1.04	15.00 ± 0.57
Pseudomonas aeruginosa	7.00 ± 0.57	8.00 ± 1.52	9.00 ± 2.51	9.33 ± 1.25	11.66 ± 2.08	12.00 ± 0.57
Streptococcus sp.	6.00 ± 2.00	8.00 ± 1.00	8.66 ± 2.08	10.00 ± 1.50	14.00 ± 0.57	15.00 ± 0.57
Escherichia coli	5.50 ± 0.86	6.00 ± 1.15	7.00 ± 1.00	9.00 ± 1.73	12.50 ± 0.86	8.00 ± 0.57

Table 5. Antibacterial activity of BA-AgNPs evaluated by agar well diffusion assay.

Biological activities

Anti-bacterial activity and spectrum confirmation

BA-AgNPs exhibited concentration-dependent antibacterial activity against one Gram-positive bacterium (*Streptococcus* sp.) and three Gram-negative strains (*E. coli*, *P. aeruginosa*, and *K. pneumoniae*) using the agar well diffusion assay (Fig. 9; Table 5). The maximum inhibition zone was observed against *Streptococcus* sp. (14 ± 0.57 mm at 0.9 mg/mL), while a smaller inhibition zone was recorded at the lowest tested concentration against *E. coli* (5.5 ± 0.86 mm at 0.1 mg/mL). These results indicate broad-spectrum antibacterial potential, with comparatively higher susceptibility of the Gram-positive strain under the tested conditions. While differences between Gram-positive and Gram-negative susceptibility are often linked to envelope architecture and permeability, activity against all tested Gram-negative strains confirms that BA-AgNPs are not restricted to Gram-positive targets and demonstrate broader antimicrobial coverage.

Minor apparent differences between the inhibition zones visible in Fig. 9 and the mean values reported in Table 5 may be due to image angle, lighting, plate positioning, and the use of representative plates in the figure. Table 5 reports the mean ± error values calculated from triplicate measurements and should therefore be considered the quantitative reference for antibacterial activity. The control wells were included to confirm assay

validity, while the concentration-dependent trend was interpreted based on replicated measurements rather than visual inspection of a single representative plate.

Comparison with previous work supports these findings. Many studies report strong antibacterial activity for green-synthesized AgNPs, with activity often increasing with concentration due to greater nanoparticle–cell contact and higher probability of membrane disruption and intracellular stress induction[60,61]. The antibacterial profile observed here is therefore consistent with established AgNP performance in microbial growth inhibition.

The present study did not experimentally probe antibacterial mechanisms (e.g., membrane leakage assays, ROS quantification, protein/DNA interaction studies). Nevertheless, the strong activity observed is plausibly explained by widely reported AgNP mechanisms, including (i) adhesion to bacterial surfaces and disruption of membrane integrity, (ii) induction of oxidative stress through ROS generation, (iii) interaction with sulfur- and phosphorus-containing biomolecules that impairs enzymatic and DNA functions, and (iv) contributions from released Ag^{+} ions that intensify antimicrobial stress. Dedicated mechanistic assays are required to validate which pathway(s) dominate for BA-AgNPs, particularly against *Streptococcus* sp., and this remains a key direction for follow-up studies.

Antioxidant activity

BA-AgNPs demonstrated notable DPPH radical scavenging activity with dose-dependent increases in inhibition (Table 6), reaching the highest scavenging at 100 ppm (88.12%), while ascorbic acid showed 80.9% at the same concentration. The observed antioxidant behavior is consistent with multiple studies reporting that green-synthesized AgNPs often exhibit radical scavenging capacity attributable to their phytochemical corona and surface functionalization[34,62–66].

Based on FTIR-confirmed functional groups and the established role of plant metabolites as capping agents, the antioxidant potential is most plausibly dominated by residual plant-derived biomolecules associated with the nanoparticle surface (e.g., phenolic compounds acting as hydrogen/electron donors). The nanoparticle surface may also contribute indirectly by facilitating electron transfer processes or stabilizing redox-active moieties; however, the current study did not include comparative controls (e.g., extract-only vs. purified/capping-removed AgNPs) to experimentally apportion the relative contribution of the metallic core versus the phytochemical corona. Thus, while antioxidant efficacy is demonstrated, the dominant source (capping layer vs. nanoparticle surface) should be resolved using targeted comparative designs in future work. Plant extract-only antioxidant controls were not included in the present DPPH assay. Therefore, the antioxidant response may reflect the combined contribution of AgNP surface activity and phytochemical capping residues. Future studies should compare crude extract, purified BA-AgNPs, and capping-removed nanoparticles to clarify the relative contribution of plant-derived compounds and the metallic nanoparticle core.

In the DPPH assay, lower absorbance at 517 nm indicates greater radical scavenging activity because more DPPH radicals are reduced by the tested sample. Therefore, the lower absorbance values observed for BA-AgNPs correspond to higher calculated inhibition percentages. The higher inhibition of BA-AgNPs compared with ascorbic acid at equivalent concentrations reflects stronger DPPH radical scavenging under the present assay conditions.

Anticancer activity

BA-AgNPs induced concentration-dependent cytotoxicity in RD cells (Table 7), with higher concentrations producing greater cell death. Similar dose-dependent anticancer effects have been reported for green-synthesized AgNPs in multiple cancer models, where nanoscale size and capping chemistry influence cellular uptake, oxidative stress induction, and apoptotic signalling[67]. The strong cytotoxicity observed may be associated with efficient nanoparticle internalization due to small particle size and high surface area, potentially enabling endocytosis and intracellular stress pathways[68–73]. Although the present work did not experimentally resolve the precise anticancer mechanism (e.g., ROS-mediated apoptosis, mitochondrial dysfunction, DNA damage), literature supports these as plausible routes for AgNP-induced cytotoxicity[74,75]. Mechanistic confirmation remains a key next step for biomedical positioning of BA-AgNPs.

Based on the concentration-dependent cytotoxicity data, BA-AgNPs produced 44.00% cell death at 6.25 mg/mL and 58.33% cell death at 12.5 mg/mL, indicating that the 50% cytotoxic response occurred between these two tested concentrations. However, the IC_{50} value was not precisely calculated because nonlinear regression analysis was not performed and additional intermediate concentrations near the 50% response level were not tested. Therefore, the IC_{50} is reported only as an estimated range of 6.25–12.5 mg/mL rather than as a single exact value.

Sample	Concentration (ppm)	BA-AgNPs absorbance	BA-AgNPs inhibition (%)	Ascorbic acid absorbance	Ascorbic acid inhibition (%)
1	10	0.452 ± 0.012	69.50 ± 1.05	1.173 ± 0.018	20.85 ± 0.96
2	20	0.421 ± 0.010	71.59 ± 0.94	1.094 ± 0.016	26.18 ± 0.88
3	40	0.358 ± 0.009	75.84 ± 0.86	0.874 ± 0.014	40.35 ± 0.91
4	50	0.349 ± 0.008	76.45 ± 0.79	0.764 ± 0.012	48.45 ± 0.85
5	75	0.278 ± 0.007	81.24 ± 0.72	0.477 ± 0.010	67.81 ± 0.80
6	100	0.176 ± 0.006	88.12 ± 0.68	0.283 ± 0.008	80.90 ± 0.74

Table 6. DPPH radical scavenging activity of BA-AgNPs compared with ascorbic acid. Values are presented as mean ± SEM from triplicate measurements.

Concentration (mg/mL)	R1	R2	R3	Mean	SD
100	87	94	80	87.00	7.00
50	71	78	87	78.67	8.02
25	57	62	71	63.33	7.09
12.5	51	57	67	58.33	8.08
6.25	44	49	39	44.00	5.00
3.125	40	36	44	40.00	4.00
1.5625	12	19	13	14.67	3.79
0.78125	6	11	15	10.67	4.51
0.39062	2	5	9	5.33	3.51

Table 7. Percent cell death (cytotoxicity, %) in RD cells treated with BA-AgNPs for 24 h.

Although BA-AgNPs showed clear concentration-dependent cytotoxicity against RD cancer cells, normal mammalian cell controls were not included in the present study. Therefore, selective anticancer efficacy and selectivity index could not be determined. The anticancer results should be interpreted only as preliminary RD-cell cytotoxic screening data rather than confirmed selective anticancer activity. Future work will include non-cancerous mammalian cell lines and extract-only treatments to evaluate biocompatibility, calculate selectivity index, and confirm whether BA-AgNPs show cancer-selective activity.

Phytotoxicity analysis and dose-dependent interpretation

Phytotoxicity of BA-AgNPs was assessed using wheat (*Triticum aestivum* var. Akbar 2019) under controlled conditions (Fig. 10). The results indicated concentration-dependent effects on growth parameters (shoot length, root length, and fresh biomass). Lower concentrations (notably 25–100 mg/L) generally produced growth-promoting trends, whereas the highest concentration (1000 mg/L) showed reduced growth compared to lower-dose groups, indicating potential toxicity at elevated exposure levels. A 75 mg/L treatment was not included in the phytotoxicity experiment because the study design focused on selected low, moderate, and high exposure levels. The reduction in root length and biomass at 100 mg/L compared with 50 mg/L suggests that the stimulatory effect of BA-AgNPs may decline beyond the optimal concentration range. This response may be associated with dose-dependent oxidative stress, altered nutrient uptake, or early phytotoxic effects at comparatively higher nanoparticle exposure.

This dose-dependent behavior aligns with broader nanoparticle–plant interaction literature, where low concentrations may stimulate growth via modulation of nutrient uptake and stress-response pathways, while higher concentrations induce oxidative stress, metabolic disturbance, or ionic toxicity[76–79]. Recent plant nanotoxicology studies further support that AgNP impacts on crop physiology are strongly dose- and surface-dependent, frequently mediated through oxidative stress responses and ion-associated signaling effects, reinforcing the importance of optimizing concentration windows for safe agricultural translation[80–84].

The beneficial effects at lower concentrations are consistent with reports where AgNPs improved growth metrics and antioxidant enzyme activity in certain crop species at controlled doses, while higher doses frequently caused inhibitory effects[85–90]. These findings emphasize that BA-AgNP application windows must be optimized carefully for agricultural relevance, and that nanoparticle dose and exposure duration are critical determinants of plant response.

Overall, BA-AgNPs exhibited nanoscale size, near-spherical morphology, crystalline fcc structure, and phytochemical-associated surface functionalization, alongside strong antibacterial (broad-spectrum), antioxidant, anticancer, and dose-dependent phytotoxic/phytomodulatory activities[91–93]. The combined evidence supports the premise that nanoscale dimensions and phytochemical capping contribute to stability and bio-interaction, thereby enhancing biological performance. However, the study has key limitations relevant to industrial translation and mechanistic completeness: (i) long-term colloidal stability under storage (e.g., DLS/zeta potential changes over weeks–months) was not assessed, (ii) batch-to-batch reproducibility of nanoparticle size distribution and biological activity was not evaluated, (iii) silver ion release kinetics into physiological media over 24 h were not measured, and (iv) mechanistic pathways underlying antimicrobial effects (e.g., ROS generation, membrane leakage, DNA/protein interaction) were not experimentally resolved. Addressing these items through stability profiling, reproducibility assessment, ion release studies, and targeted mechanistic assays will be necessary to strengthen validation for scale-up and biomedical/industrial deployment.

If BA-AgNPs are incorporated into polymeric coatings or films for industrial applications (e.g., antimicrobial packaging, medical-device surfaces, or high-touch coatings), controlling silver ion leaching is essential to maintain efficacy while minimizing environmental loading. In practice, Ag^+ release can be moderated by immobilizing AgNPs within crosslinked polymer matrices, applying multilayer/barrier architectures, or using encapsulation/embedding strategies (e.g., sol–gel, nanocomposite films) that reduce burst release and enable sustained, interface-localized activity. Such design approaches can preserve antimicrobial performance by maintaining a low, sustained Ag^+ flux at the surface while limiting bulk diffusion into surrounding media. Although Ag^+ release kinetics were not quantified in the present study, future translational work should combine standardized leaching tests in relevant media with performance retention assays to establish durability, safety, and environmental compatibility of BA-AgNP-enabled coatings.

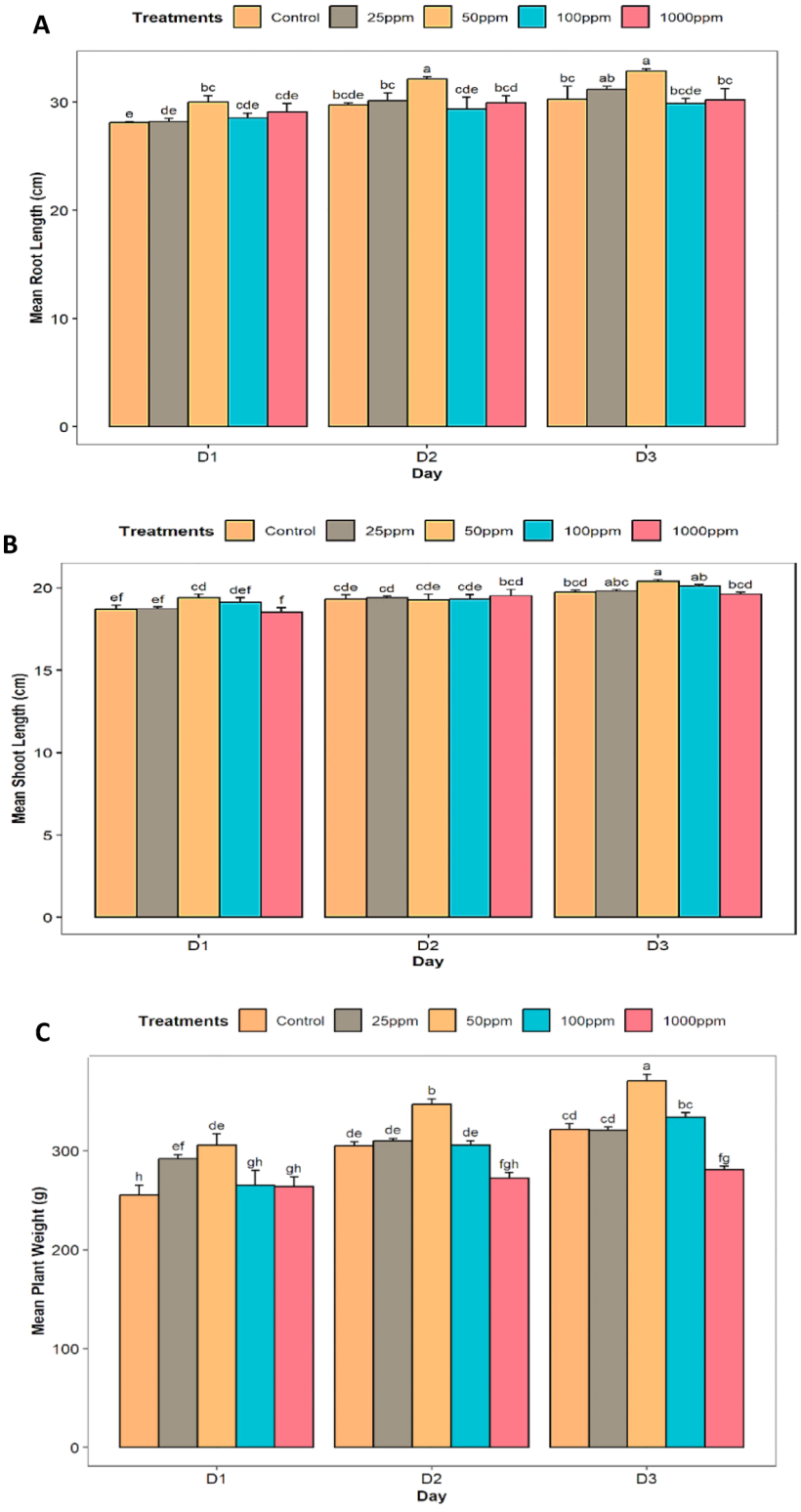

Fig. 10. Phytotoxicity assay in wheat (*Triticum aestivum* var. Akbar 2019) showing dose-dependent effects of BA-AgNPs on seedling growth parameters: (**A**) root length, (**B**) shoot length, and (**C**) fresh biomass. Different lowercase letters above bars indicate statistically significant differences among treatments at $p < 0.05$.

Conclusions

Buddleja asiatica leaf extract enabled a simple green route for synthesizing BA-AgNPs with confirmed nanoscale formation (SPR band at 400–500 nm), crystalline fcc structure by XRD, near-spherical morphology by SEM, silver predominance by EDX, phytochemical surface functionalization by FTIR, and a moderately negative

zeta potential (−18.7 mV) indicative of initial colloidal stability. The BA-AgNPs exhibited broad-spectrum antibacterial activity against both Gram-positive (*Streptococcus* sp.) and Gram-negative (*E. coli, P. aeruginosa,* and *K. pneumoniae*) strains, significant antioxidant potential in the DPPH assay, concentration-dependent cytotoxicity against RD cancer cells, and concentration-dependent effects on wheat growth with lower doses showing growth-promoting trends and the highest dose indicating phytotoxicity. Collectively, these findings suggest that BA-AgNPs have promising antibacterial, antioxidant, anticancer, and dose-dependent phytotoxic/phytomodulatory potential. However, the results should be interpreted as preliminary because normal-cell cytotoxicity controls, nonlinear regression-based IC_{50} determination, long-term stability testing, batch reproducibility, silver ion release kinetics, and detailed mechanistic assays were not performed; consequently, the IC_{50} is reported only as an estimated range of 6.25–12.5 mg/mL, not as a precisely calculated value. Further validation is therefore required before confirming biomedical, agricultural, or industrial applicability.

Data availability

The author confirms that all data generated or analyzed during this study are included in this published article.

Received: 30 March 2026; Accepted: 10 June 2026
Published online: 30 July 2026

References

1. Frewer, L. J. et al. Consumer attitudes towards nanotechnologies applied to food production. *Trends Food Sci. Technol.* **40**, 211–225 (2014).
2. Vélez, M. A., Perotti, M. C., Santiago, L., Gennaro, A. M. & Hynes, E. Bioactive compounds delivery using nanotechnology: design and applications in dairy food. In *Nutrient Delivery* 221–250 (Academic Press, 2017).
3. Mohanpuria, P., Rana, N. K. & Yadav, S. K. Biosynthesis of nanoparticles: technological concepts and future applications. *J. Nanopart. Res.* **10**, 507–517 (2008).
4. Rafique, M., Sadaf, I., Rafique, M. S. & Tahir, M. B. A review on green synthesis of silver nanoparticles and their applications. *Artif. Cells Nanomed. Biotechnol.* **45**, 1272–1291 (2017).
5. Angulo-Pineda, C. et al. Antibacterial silver nanoparticles supported on graphene oxide with reduced cytotoxicity. *JOM* **71**, 3698–3705 (2019).
6. Foldbjerg, R., Dang, D. A. & Autrup, H. Cytotoxicity and genotoxicity of silver nanoparticles in the human lung cancer cell line A549. *Arch. Toxicol.* **85**, 743–750 (2011).
7. Wypij, M. et al. Green synthesized silver nanoparticles: antibacterial and anticancer activities, biocompatibility, and analyses of surface-attached proteins. *Front. Microbiol.* **12**, 632505 (2021).
8. Karmous, I., Pandey, A., Haj, K. B. & Chaoui, A. Efficiency of the green synthesized nanoparticles as new tools in cancer therapy: insights on plant-based bioengineered nanoparticles, biophysical properties, and anticancer roles. *Biol. Trace Elem. Res.* **196**, 330–342 (2020).
9. Kim, K. J. et al. Antifungal activity and mode of action of silver nano-particles on *Candida albicans*. *Biometals* **22**, 235–242 (2009).
10. Adhikari, A. et al. Green synthesis of silver nanoparticles using *Artemisia vulgaris* extract and its application toward catalytic and metal-sensing activity. *Inorganics* **10**, 113 (2022).
11. Nayak, D., Ashe, S., Rauta, P. R., Kumari, M. & Nayak, B. Bark extract mediated green synthesis of silver nanoparticles: Evaluation of antimicrobial activity and antiproliferative response against osteosarcoma. *Mater. Sci. Eng. C* **58**, 44–52 (2016).
12. Ojemaye, M. O., Okoh, S. O. & Okoh, A. I. Silver nanoparticles (AgNPs) facilitated by plant parts of *Crataegus ambigua* Becker AK extracts and their antibacterial, antioxidant and antimalarial activities. *Green Chem. Lett. Rev.* **14**, 51–61 (2021).
13. Ajitha, B., Ahn, C. W., Yadav, P. K. & Reddy, Y. A. K. Silver nanoparticle embedded polymethacrylic acid/polyvinylpyrrolidone nanofibers for catalytic application. *J. Environ. Chem. Eng.* **9**, 106291 (2021).
14. Jiang, C., Bai, Z., Yuan, F., Ruan, Z. & Wang, W. A colorimetric sensor based on glutathione-AgNPs as peroxidase mimetics for the sensitive detection of thiamine (vitamin B1). *Spectrochim. Acta A Mol. Biomol. Spectrosc.* **265**, 120348 (2022).
15. Zhao, Y. et al. Speciation, controlling steps and pathways of silver release from the sludge generated from coagulation of wastewater spiked with silver nanoparticles. *Chemosphere* **282**, 131093 (2021).
16. Chaudhuri, S. K., Chandela, S. & Malodia, L. Plant-mediated green synthesis of silver nanoparticles using *Tecomella undulata* leaf extract and their characterization. *Nano Biomed. Eng.* **8**, 1 (2016).
17. Gudikandula, K. & Charya Maringanti, S. Synthesis of silver nanoparticles by chemical and biological methods and their antimicrobial properties. *J. Exp. Nanosci.* **11**, 714–721 (2016).
18. Lu, J. Y. et al. Facile microwave-assisted synthesis of Sb2O3-CuO nanocomposites for catalytic degradation of p-nitrophenol. *J. Mol. Liq.* **409**, 125503. https://doi.org/10.1016/j.molliq.2024.125503 (2024).
19. Salunke, B. K., Sathiyamoorthi, E., Tran, T. K. & Kim, B. S. Phyto-synthesized silver nanoparticles for biological applications. *Korean J. Chem. Eng.* **34**, 943–951 (2017).
20. Wu, B., Wang, Z., Xie, H. & Xie, P. Dimethyl fumarate augments anticancer activity of Ångstrom silver particles in myeloma cells through NRF2 activation. *Adv. Ther.* **8**, 2400363. https://doi.org/10.1002/adtp.202400363 (2025).
21. Wu, J. et al. A cost-effective and sensitive voltammetric sensor for determination of baicalein in herbal medicine based on shuttle-shape α-Fe2O3 nanoparticle decorated multi-walled carbon nanotubes. *Colloids Surf. A Physicochem. Eng. Asp.* **717**, 136850. https://doi.org/10.1016/j.colsurfa.2025.136850 (2025).
22. Khan, S., Ullah, H. & Zhang, L. Bioactive constituents from *Buddleja* species. *Pak. J. Pharm. Sci.* **32**, 2 (2019).
23. Lee, S., Xiao, C. & Pei, S. Ethnobotanical survey of medicinal plants at periodic markets of Honghe Prefecture in Yunnan Province. *SW China. J. Ethnopharmacol.* **117**, 362–377 (2008).
24. Nafees, M., Barkatullah, Ullah, S. & Ikram, N. Phytochemical and pharmacognostic studies of *Buddleja asiatica* leaves. *Microsc. Res. Tech.* **85**, 510–520 (2022).
25. Cuevas-Cianca, S. I., Leal, A. C. L., Hernández, L. R., Arreola, E. S. & Bach, H. Antimicrobial, toxicity, and anti-inflammatory activities of *Buddleja perfoliata* Kunth. *Phytomedicine Plus* **2**, 100357 (2022).
26. Mohamed, M., Abdou, A., Saad, A. & Ibrahim, M. Cytotoxic activity of *Buddleja asiatica*. *Life Sci. J.* **10**, 2773–2777 (2013).
27. Ali, S. S. M., Aljawobaei, W., Rao, V. J., Nagar, P. S. & Robin, P. Sustainable synthesis of silver nanoparticles using *Barleria prattensis* extract: Characterization and evaluation of their biological and catalytic activities. *Biomass Convers. Biorefin.* **15**, 17811–17828. https://doi.org/10.1007/s13399-024-06374-8 (2025).
28. Ali, S. S. M., Dawale, A. M. A., Samal, S., Robin, P. & Thakore, S. *Barleria grandiflora* leaf extract-driven silver nanoparticles: Assessment of their antibacterial, cytotoxicity, and catalysis. *ChemistrySelect* **10**, e00764. https://doi.org/10.1002/slct.202500764 (2025).
29. Ali, S. S. M. et al. Ecofriendly synthesis of silver nanoparticles using *Barleria gibsonii* and evaluation of antibacterial antioxidant cytotoxic and catalytic activities. *Sci. Rep.* **16**, 8281. https://doi.org/10.1038/s41598-026-37330-3 (2026).

30. Mohsen Ali, S. S. & Robin, P. Comprehensive phytochemical profiling of bioactive compounds from *Barleria prattensis* for their antioxidant and cytotoxic capacity and its characterization using GC-MS. *Biochem. Biophys. Rep.* **43**, 102083. https://doi.org/10.1016/j.bbrep.2025.102083 (2025).
31. Das, S., Kalita, M. C. & Shukla, S. Rapid biosynthesis of silver nanoparticles using leaf extract of *Brassica oleracea* var. *gongylodes* and their antimicrobial activity. *World J. Pharm. Pharm. Sci.* **7**, 1135–1145 (2018).
32. Yan, H. et al. Breaking the selectivity dilemma: a 114-fold bee-safe AIE nanoinsecticide via spontaneous non-covalent orchestration. *Chem. Eng. J.* **529**, 172939. https://doi.org/10.1016/j.cej.2026.172939 (2026).
33. Khalil, S. et al. Antibacterial, antioxidant and photocatalytic activity of novel *Rubus ellipticus* leaf mediated silver nanoparticles. *J. Saudi Chem. Soc.* **27**, 101576 (2023).
34. Zulfiqar, H. et al. Antibacterial, antioxidant, and phytotoxic potential of phytosynthesized silver nanoparticles using *Elaeagnus umbellata* fruit extract. *Molecules* **27**, 5847 (2022).
35. Anandalakshmi, K., Venugobal, J. & Ramasamy, V. Characterization of silver nanoparticles by green synthesis method using *Pedalium murex* leaf extract and their antibacterial activity. *Appl. Nanosci.* **6**, 399–408 (2016).
36. Moharram, A. H., Mansour, S. A., Hussein, M. A. & Rashad, M. Direct precipitation and characterization of ZnO nanoparticles. *J. Nanomater.* **2014**, 716210 (2014).
37. Baudot, C., Tan, C. M. & Kong, J. C. FTIR spectroscopy as a tool for nano-material characterization. *Infrared Phys. Technol.* **53**, 434–438 (2010).
38. Nagarajan, S., Kalaivani, G., Poongothai, E., Arul, M. & Natarajan, H. Characterization of silver nanoparticles synthesized from *Catharanthus roseus* (*Vinca rosea*) plant leaf extract and their antibacterial activity. *IJRAR* **6**, 680–685 (2019).
39. Silva, L. P., Pereira, T. M. & Bonatto, C. C. Frontiers and perspectives in the green synthesis of silver nanoparticles. In *Green Synthesis, Characterization and Applications of Nanoparticles* 137–164 (Academic Press, 2019).
40. Nanda, A. & Saravanan, M. Biosynthesis of silver nanoparticles from *Staphylococcus aureus* and its antimicrobial activity against MRSA and MRSE. *Nanomedicine* **5**, 452–456 (2009).
41. Ovais, M. et al. HPLC-DAD finger printing, antioxidant, cholinesterase, and α-glucosidase inhibitory potentials of a novel plant *Olax nana*. *BMC Complement. Altern. Med.* **18**, 1 (2018).
42. Lyons, B. W., Wu, L. L., Astill, M. E. & Wu, J. T. Development of an assay for modulating anti-acetylcholine receptor autoantibodies using human rhabdomyosarcoma cell line. *J. Clin. Lab. Anal.* **12**, 315–319 (1998).
43. Baran, M. F. Green synthesis of silver nanoparticles using *Pistacia terebinthus* leaf extract: antimicrobial effect and characterization. *Int. J. Math. Sci.* **2602**, 5 (2018).
44. Gharari, Z., Hanachi, P., Sadeghinia, H. & Walker, T. R. Eco-friendly green synthesis and characterization of silver nanoparticles by *Scutellaria multicaulis* leaf extract and its biological activities. *Pharmaceuticals* **16**, 992 (2023).
45. Shameli, K. et al. Green biosynthesis of silver nanoparticles using *Callicarpa maingayi* stem bark extraction. *Molecules* **17**, 8506–8517 (2012).
46. Labulo, A. H., David, O. A. & Terna, A. D. Green synthesis and characterization of silver nanoparticles using *Morinda lucida* leaf extract and evaluation of its antioxidant and antimicrobial activity. *Chem. Pap.* **76**, 7313–7325 (2022).
47. Aref, M. S. & Salem, S. S. Bio-callus synthesis of silver nanoparticles, characterization, and antibacterial activities via *Cinnamomum camphora* callus culture. *Biocatal. Agric. Biotechnol.* **27**, 101689 (2020).
48. Almatroudi, A. et al. Antibacterial, antibiofilm and anticancer activity of biologically synthesized silver nanoparticles using seed extract of *Nigella sativa*. *Processes* **8**, 388 (2020).
49. Rahimi-Nasrabadi, M., Pourmortazavi, S. M., Shandiz, S. A. S., Ahmadi, F. & Batooli, H. Green synthesis of silver nanoparticles using *Eucalyptus leucoxylon* leaves extract and evaluating the antioxidant activities of extract. *Nat. Prod. Res.* **28**, 1964–1969 (2014).
50. Castro-Longoria, E., Vilchis-Nestor, A. R. & Avalos-Borja, M. Biosynthesis of silver, gold and bimetallic nanoparticles using the filamentous fungus *Neurospora crassa*. *Colloids Surf. B Biointerfaces* **83**, 42–48 (2011).
51. Kartini, K. et al. Process optimization for green synthesis of silver nanoparticles using Indonesian medicinal plant extracts. *Processes* **8**, 998 (2020).
52. Rafique, M. et al. Novel and facile synthesis of silver nanoparticles using *Albizia procera* leaf extract for dye degradation and antibacterial applications. *Mater. Sci. Eng. C* **99**, 1313–1324 (2019).
53. Talib, H. et al. Antibacterial, antioxidant, and anticancer potential of green fabricated silver nanoparticles made from *Viburnum grandiflorum* leaf extract. *Bot. Stud.* **65**, 4 (2024).
54. Carson, L. et al. Green synthesis of silver nanoparticles with antimicrobial properties using *Phyla dulcis* plant extract. *Foodborne Pathog. Dis.* **17**, 504–511 (2020).
55. Barapatre, A., Aadil, K. R. & Jha, H. Synergistic antibacterial and antibiofilm activity of silver nanoparticles biosynthesized by lignin-degrading fungus. *Bioresour. Bioprocess.* **3**, 1–13 (2016).
56. Hanachi, P., Gharari, Z., Sadeghinia, H. & Walker, T. R. Synthesis of bioactive silver nanoparticles with eco-friendly processes using *Heracleum persicum* stem extract and evaluation of their antioxidant, antibacterial, anticancer and apoptotic potential. *J. Mol. Struct.* **1265**, 133325 (2022).
57. Saleh Alkarri, Z., Bashir, Z., Wimmer, M., Schorzmann, J. & Döpper, F. Anti-microbial plastic parts fabricated by high-speed sintering. *Mater. Sci. Addit. Manuf.* **3**, 4970. https://doi.org/10.36922/msam.4970 (2024).
58. Wang, F. et al. Simultaneous suppression of As mobilization and N2O emission from NH4+/As-rich paddy soils by combined nitrate and birnessite amendment. *J. Hazard. Mater.* **465**, 133451. https://doi.org/10.1016/j.jhazmat.2024.133451 (2024).
59. Zhang, Y. et al. Fabrication of metastable nanoscale Ag-Cu supersaturated solid solutions and their low-temperature low-pressure interconnect applications. *J. Mater. Sci. Technol.* **246**, 76–85. https://doi.org/10.1016/j.jmst.2025.04.066 (2026).
60. Bapat, R. A. et al. An overview of application of silver nanoparticles for biomaterials in dentistry. *Mater. Sci. Eng. C* **91**, 881–898 (2018).
61. Khorrami, S., Zarrabi, A., Khaleghi, M., Danaei, M. & Mozafari, M. R. Selective cytotoxicity of green synthesized silver nanoparticles against the MCF-7 tumor cell line and their enhanced antioxidant and antimicrobial properties. *Int. J. Nanomedicine* **13**, 8013–8024 (2018).
62. Bahrun, A. H. et al. A novel approach to evaluate the interaction effects of nano silica bokashi fertilizer on several rice varieties using multivariate analysis. *Int. J. Agric. Biosci.* **14**, 136–144 (2025).
63. Khang, T. N., Binh, H. T., Dao, V. T. T., Thao, L. T. T. & Duy, T. T. Antibacterial and antifungal abilities of *Tacca leontopetaloides* L. Kuntze leaf extraction and its application in fresh mango preservation. *Int. J. Agric. Biosci.* **14**, 556–564 (2025).
64. Nagaich, U., Gulati, N. & Chauhan, S. Antioxidant and antibacterial potential of silver nanoparticles: biogenic synthesis utilizing apple extract. *J. Pharm.* **2016**, 7141523 (2016).
65. Pradiza, R. R. et al. Morphology and tensile properties of biocomposite based polyvinyl alcohol and cassava starch reinforced by lemon peel fiber. *Int. J. Agric. Biosci.* **14**, 549–555 (2025).
66. Rueangsri, K., Lasunon, P., Kwantrairat, S. & Taweejun, N. Effect of ultrasound-assisted aqueous two-phase extraction on phenolic compounds from *Nymphaea pubescens* Willd. and its antioxidant and antimicrobial properties. *Int. J. Agric. Biosci.* **14**, 1–10 (2025).
67. Hublikar, L. V., Ganachari, S. V., Patil, V. B., Nandi, S. & Honnad, A. Anticancer potential of biologically synthesized silver nanoparticles using *Lantana camara* leaf extract. *Prog. Biomater.* **12**, 155–169 (2023).
68. Amin, N. U. et al. Allelopathic effect of sunflower on crops and pathogens. *Trends Anim. Plant Sci.* **4**, 39–44 (2024).
69. Halder, J., Pradhan, D., Kar, B., Ghosh, G. & Rath, G. Nanotherapeutics approaches to overcome P-glycoprotein-mediated multi-drug resistance in cancer. *Nanomedicine* **40**, 102494 (2022).

70. Haq, I. U. Harnessing nanotechnology for superior fruit crop quality and yield enhancement. *Trends Anim. Plant Sci.* **4**, 74–81 (2024).
71. Ihsan, M. et al. Allelopathy of *Parthenium hysterophorus* L. on lettuce, wheat and selected pathogens. *Trends Anim. Plant Sci.* **4**, 30–38 (2024).
72. Mahmood, Q., Shaheen, S. & Azeem, M. Nanobiosensors: application in healthcare, environmental monitoring and food safety. *Asian J. Agric. Biol.* **2024**, 2023157 (2024).
73. Ullah, R. The therapeutic potential of aromatic plants: a new frontier in bioactive compound research. *Trends Anim. Plant Sci.* **4**, 112–117 (2024).
74. He, Z. et al. Reactive oxygen species (ROS): utilizing injectable antioxidative hydrogels and ROS-producing therapies to manage the double-edged sword. *J. Mater. Chem. B* **9**, 6326–6346 (2021).
75. Xu, L. et al. Genotoxicity and molecular response of silver nanoparticle (NP)-based hydrogel. *J. Nanobiotechnol.* **10**, 1–11 (2012).
76. Lin, D. & Xing, B. Phytotoxicity of nanoparticles: inhibition of seed germination and root growth. *Environ. Pollut.* **150**, 243–250. https://doi.org/10.1016/j.envpol.2007.01.016 (2007).
77. Mahawar, H. & Prasanna, R. Prospecting the interactions of nanoparticles with beneficial microorganisms for developing green technologies for agriculture. *Environ. Nanotechnol. Monit. Manag.* **10**, 477–485. https://doi.org/10.1016/j.enmm.2018.09.004 (2018).
78. Rizwan, M. et al. Effect of metal and metal oxide nanoparticles on growth and physiology of globally important food crops: a critical review. *J. Hazard. Mater.* **322**, 2–16. https://doi.org/10.1016/j.jhazmat.2016.05.061 (2017).
79. Ruttkay-Nedecký, B., Kryštofová, O., Nejdl, L. & Adam, V. Nanoparticles based on essential metals and their phytotoxicity. *Nanoscale Res. Lett.* https://doi.org/10.1186/s12951-017-0268-3 (2017).
80. Ahmad, S. et al. Nutrient strengthening and stress alleviation in rice (*Oryza sativa* L.) via foliar ceria nanoparticles and biochar amendment under elevated CO_2-mediated warming. *Plant Physiol. Biochem.* **229**, 110364 (2025).
81. Altaf, S. et al. Tailored nanoparticles in precision animal and human oncology: engineering tumor-selective delivery and microenvironment interplay. *Agrobiol. Rec.* **22**, 61–72 (2025).
82. Mehwish, Azam, S. E. & Muzamail, S. Unveiling the future: nanotechnology's role in advanced food packaging. *Agrobiol. Rec.* **15**, 24–33 (2024).
83. Shoukat, A. Nanofertilizers and stress management: emerging opportunities for climate-resilient farming. *Agrobiol. Rec.* **22**, 73–88 (2025).
84. Usman, M. et al. Sustainable synthesis of silver nanoparticles using *Moringa oleifera* leaf extract and assessment of antibacterial efficacy. *Agrobiol. Rec.* **21**, 147–153 (2025).
85. Ahsan, H. et al. Efficacy of silver oxide nanoparticles against multi-drug resistant *Pseudomonas aeruginosa* and methicillin-resistant *Staphylococcus aureus* in burn wound infections. *Asian J. Agric. Biol.* **2024**, 2024096 (2024).
86. Pallavi, C. M., Mehta, R., Srivastava, R., Arora, S. & Sharma, A. K. Impact assessment of silver nanoparticles on plant growth and soil bacterial diversity. *3 Biotech* https://doi.org/10.1007/s13205-16-0567-7 (2016).
87. Pham-Khanh, N. H., Huynh, N. Q., Le, H. N. B. & Ha, T. K. Q. Green synthesis of zinc oxide microparticles using the leaf extract of *Dolichandrone spathacea* in sustainable agriculture: a new approach for protecting the legume plant (*Vigna radiata*) against the Cr(VI) stress. *Asian J. Agric. Biol.* **2024**, 2023245 (2024).
88. Rasool, M., Rasool, M. H., Khurshid, M. & Aslam, B. Biogenic synthesis and characterization of silver nanoparticles: exploring antioxidant and anti-inflammatory activities and assessing antimicrobial potential against multidrug-resistant bacteria. *Asian J. Agric. Biol.* **2024**, 2023364 (2024).
89. Tomacheski, D., Pittol, M., Simões, D. N., Ribeiro, V. F. & Santana, R. M. C. Impact of silver ions and silver nanoparticles on plant growth and soil microorganisms. *Glob. J. Environ. Sci. Manag.* **3**, 341–350. https://doi.org/10.22034/gjesm.2017.03.04.001 (2017).
90. Tymoszuk, A. Silver nanoparticles effects on in vitro germination, growth, and biochemical activity of tomato, radish, and kale seedlings. *Materials* **14**, 5340. https://doi.org/10.3390/ma14185340 (2021).
91. Wang, X. et al. Carrier-free nanoparticles based on natural products trigger dual "synergy and attenuation" for enhanced phototherapy of liver cancer. *Mater. Today Bio* **35**, 102278. https://doi.org/10.1016/j.mtbio.2025.102278 (2025).
92. Zeng, J. et al. Biomimetic ginsenoside Rb1 and probucol co-assembled nanoparticles for targeted atherosclerosis therapy via inhibition of oxidative stress, inflammation, and lipid deposition. *ACS Nano* **19**, 22968–22987. https://doi.org/10.1021/acsnano.5c02492 (2025).
93. Zu-Man, D. et al. Construction of blackberry polysaccharide nano-selenium particles: structure features and regulation effects of glucose/lipid metabolism in HepG2 cells. *Food Res. Int.* **187**, 114428. https://doi.org/10.1016/j.foodres.2024.114428 (2024).

Acknowledgements

This work was supported by Deanship of Scientific Research, Vice Presidency for Graduate Studies and Scientific Research, King Faisal University, Saudi Arabia (KFU263490).

Author contributions

MF, MSA, AM, SK, ZB, HA, HQ, TA: methodology, supervision, experimentation, data curation, writing, drafting, and research design, data collection, validation, software, writing, investigation, drafting, statistical analysis; HSEB, IMA, KHA, NYR, MAS: writing, software, resource, research design, validation, drafting, statistical analysis. All authors reviewed the manuscript.

Funding

This work was supported by Deanship of Scientific Research, Vice Presidency for Graduate Studies and Scientific Research, King Faisal University, Saudi Arabia (KFU263490).

Declarations

Competing interests

The authors declare no competing interests.

Ethics approval and consent to participate

This article does not contain any studies on human or animal subjects. The current experimental research and field study including the collection of plant material, is complying with relevant institutional, national, and international guidelines and legislation and used for research and development.

Additional information

Correspondence and requests for materials should be addressed to T.A., H.S.E.-B. or M.A.S.

Reprints and permissions information is available at www.nature.com/reprints.

Publisher's note Springer Nature remains neutral with regard to jurisdictional claims in published maps and institutional affiliations.

Open Access This article is licensed under a Creative Commons Attribution-NonCommercial-NoDerivatives 4.0 International License, which permits any non-commercial use, sharing, distribution and reproduction in any medium or format, as long as you give appropriate credit to the original author(s) and the source, provide a link to the Creative Commons licence, and indicate if you modified the licensed material. You do not have permission under this licence to share adapted material derived from this article or parts of it. The images or other third party material in this article are included in the article's Creative Commons licence, unless indicated otherwise in a credit line to the material. If material is not included in the article's Creative Commons licence and your intended use is not permitted by statutory regulation or exceeds the permitted use, you will need to obtain permission directly from the copyright holder. To view a copy of this licence, visit http://creativecommons.org/licenses/by-nc-nd/4.0/.

© The Author(s) 2026